https://doi.org/10.1016/j.jclepro.2019.02.137

Approaching low-energy high-rise building by integrating passive architectural design with photovoltaic application

Xi Chen [a*], Junchao Huang [a], Hongxing Yang [a] and Jinqing Peng [b]

[a] Renewable Energy Research Group (RERG), Department of Building Services Engineering, The Hong Kong Polytechnic University, Kowloon, Hong Kong, China
[b] College of Civil Engineering, Hunan University, Changsha 410082, Hunan, China

Abstract

Building envelopes can highly impact the building energy demand and indoor environmental quality, so that the application of novel façade systems such as photovoltaics has been widely investigated. However, few study has addressed the interactive effect between photovoltaic (PV) application and traditional passive architectural design strategies, which is thoroughly discussed in this comparative study using a holistic design optimization process. The holistic design optimization approach combines screening-based and variance-based sensitivity analyses with the non-dominated sorting genetic algorithm-II (NSGA-II) and hybrid generalized pattern search particle swarm optimization (HGPSPSO). The impact of the light-to-solar gain ratio (LSG) is evaluated as one of the key factor to combine the passive design and PV glazing based on a comprehensive glazing database. Through an exhaustive sensitivity analysis (SA), the Morris method is proved to be efficient and robust in factor prioritizing only when the required minimum sampling size is satisfied. The window to ground ratio showed much greater impact on the net building energy demand when PV applications are coupled with all available vertical façades. Furthermore, the necessary particles for specified design input dimensions are determined for the optimal performance of HGPSPSO. With the optimum design configuration, the net building demand can be reduced by up to 71.36% under the hot summer and warm winter condition of Hong Kong. Research findings from this study can be used to develop low-energy building guidelines and building integrated PV applications in early planning stages.

Keywords: Photovoltaic application; Low-energy building; Passive design; Sensitivity analysis; Particle swarm optimization

* Corresponding author: Tel.:+852-2766 4726, Fax: 2765 7198, E-mail: climber027@gmail.com

Nomenclatures

Abbreviation	
BEAM	building environment assessment method
BO	building orientation
COP	coefficient of performance
FAST	Fourier amplitude sensitivity test
GPVA	active glazing PV area
GPS	generalized pattern search
HGPSPSO	hybrid generalized pattern search particle swarm optimization
HVAC	heating ventilation and air conditioning
IACH	infiltration air change per hour
IWEC	international weather for energy calculations
LSG	light to solar gain ratio
NSGA-II	non-dominated sorting genetic algorithm-II
OPF	overhang projection fraction
PSO	particle swarm optimization
PV	photovoltaic
SA	sensitivity analysis
SHGC	solar heat gain coefficient
VT	visible transmittance
WGR	window to ground ratio
WOF	window opening factor
WPVA	active wall PV area
WSH	wall specific heat
WTR	wall thermal resistance
WU	window U-value

1. Introduction

Building energy and indoor environmental performances are critical in modern society as buildings are main energy consumers and people spend most of their time on interior activities (Zhou et al., 2018). In densely populated mega-city like Hong Kong, more than 30% of local residents lives in modularly designed high-rise residential buildings where envelope designs are crucial for improving their energy efficiency and indoor environmental quality (Mirrahimi et al., 2016). In the latest version of the green building assessment scheme in Hong Kong, passive design and integrated renewable systems (especially Photovoltaics) are both considered effective strategies to improve the envelope design. Some recent application of these two strategies in building sensitivity analyses and optimization studies are briefly outlined as below.

Passive architectural design strategies are constantly under the spotlight because of their low initial costs and validated competence in improving building performance (Pal et al., 2017). Up to ten key passive architectural design parameters are identified from existing literatures and their impact on building performance has been confirmed by robust sensitivity analyses based on modelling

experiments (Chen et al., 2017b). In these parametric studies, the ratio between the visible light transmittance (VT) and the solar heat gain coefficient (SHGC), namely the light-to-solar gain ratio (LSG), is usually assumed to be around 1.0 or restricted to a discrete distribution (Delgarm et al., 2016; Zhang et al., 2017). Therefore, the whole possible distribution range of LSG and its influence over the building performance cannot be accurately quantified. As shown in Fig. 1, LSG of miscellaneous glazing could be lower than 0.5 for tinted glass or higher than 2.0 for selective insulative glass (Szabó, 2015). The concept of separating solar heat gain and daylight performance is important when assessing the impact of window configurations on indoor thermal and visual conditions. Discrete LSGs between 1.0 and 1.8 were modelled by independently varying SHGC and VT to investigate the spatial and temporal indoor environment of a typical classroom design (Zomorodian and Tahsildoost, 2017). Windows with high LSG can alleviate the trade-off between indoor thermal and daylight optimization objectives in hot climates, where a maximum energy saving up to 33% can be achieved by adopting window systems with LSG between 1.09 and 2.24 (Lee and Won, 2017; Lee et al., 2013).

Apart from passive architectural design, building integrated photovoltaics (BIPV) is another innovative envelope design to improve the overall building performance and outlook (Skandalos and Karamanis, 2015). Building energy efficiency and thermal comfort was subject to a Parameterized Cognitive Adaptive Optimization based on both model-based and model-free control strategy (Baldi et al., 2015b). The proposed optimization control strategy was proved to be more effective in improving building performances, and was then applied to the whole micro-grid minimized the net energy absorption from the power grid (Baldi et al., 2015a). Opaque PV envelopes with mono-crystalline silicon cells were also optimized with the genetic algorithm to reduce building energy costs and increase PV utilization (Youssef et al., 2016). In this study, different building shapes and widow to wall ratios are tested for designing the net-zero energy building in Egypt. On top of coupling PV with opaque walls, semi-transparent photovoltaic (STPV) glazing is attracting extensive attention due to its greater contribution to heat gain reduction and advantage in daylight modulation. It is estimated that PV glazing can reduce envelope heat gain in a range from 13.59% to 38.78% (Chan, 2018), so that its effect should be considered in the evaluation of Overall Thermal Transfer Value in Hong Kong. STPV is proved to reduce overall building energy consumption compared with double-

pane clear, low-E and traditional single clear glazing by evaluating both daylight and thermal performances (Zhang et al., 2016). Furthermore, the overall energy efficiency of crystalline and amorphous PV glazing is optimized by varying the covering ratio and building orientation while keeping a reasonable level of visual comfort (Skandalos et al., 2018). Preliminary sensitivity analyses are also conducted on variable PV glazing materials with different window geometric, thermal and optical features, and their energy conservation potential in different climates has been discussed (Gueymard and duPont, 2009; Lee et al., 2014).

Based on the above background study, most existing research mainly focuses on the design optimization of traditional passive architectural design parameters, while the characteristics of envelope photovoltaic (PV) applications are seldom incorporated into the whole process. The optimization of semi-transparent PV applications is usually limited to window orientation and physical properties, whereas other correlated design factors such as the window to ground ratio (i.e. the total area of the window divided by the total area of the floor), ventilation opening area, infiltration rate, local shadings and external obstructions are not sufficiently addressed. Therefore, this paper fills such research gaps by investigating the interactive effect when incorporating PV facades with significant architectural design parameters to explore the potential of near-zero energy high-rise residential buildings. Major contributions lie in the following aspects: (1) Dependent variables including the solar heat gain coefficient, window opening factors and active glazing/wall PV areas are dynamically coupled with independent design architectural design factors such as visible transmittance, light-to-solar gain ratio and window to ground ratio; (2) The minimum required sampling and search agent size (number of particles) for the sensitivity analysis and optimization is clarified for different design input dimensions to improve the robustness of the statistical interpretation, while bootstrapping-based quantitative sensitivity indices are introduced to curtail the design input dimension; (3) A post-Pareto analysis revealed the underlying statistical structure of design input configurations, where a widely spread design variable in its definition domain was proved to indicate its insignificance rather than its importance in the optimization process; (4) The parametric analysis and design optimization is closely correlated with green building criteria in energy and indoor environment, so that the adopted research methodology can be used for benchmarking and resource deployment in developing sustainable new constructions..

For the rest of this paper, Section 2 details the research framework and methodology to conduct the holistic design optimization on a hybrid-ventilated and dimming-controlled residential prototype model; Section 3 presents in-depth result analyses and discussions on the sensitivity study, Pareto-based multi-criterion optimization, the final optimum solution and its impact on building performance indicators; Section 4 then summarizes the main finding in this research.

2. Research design and methodology

The framework of adopted research methodologies is briefly illustrated in Fig. 2. Both traditional independent passive design factors and corresponding dependent PV envelope parameters are first specified in the EnergyPlus model with prescribed distribution functions. Monte Carlo sampling, widely used in modelling experiments as an approach to multidimensional integrals (Robert and Casella, 2004), is then conducted to generate input-output matrices through JEPlus. Both qualitative (Morris) and quantitative (FAST) sensitivity analyses are conducted with R programming and the adequate sampling size for Morris is determined to generate consistent factor prioritizing results with FAST. Bootstrapped total-order indices are used to reduce the design problem space for subsequent optimizations (Chen et al., 2017a). Both NSGA-II and HGPSPSO in GenOpt are adopted to deliver Pareto optima and final optimum solutions for design scenarios with and without PV systems (Delgarm et al., 2016; Méndez Echenagucia et al., 2015). In addition, the minimum required particle number (i.e. the swarm size for PSO) as well as detailed energy and indoor environmental performance of optimum solutions will be discussed in detail. Specification for each research method is further elaborated and justified in below sessions.

2.1.Determination of design input and building modelling

2.1.1. Weather conditions

As mentioned in the introduction session, the spectrum selective glazing with high LSG is more suitable for cooling dominated climates considering both indoor thermal and daylight performance. Therefore, the weather data in the format of IWEC (International Weather for Energy Calculations) is used to study the annual building performance under hot and humid climatic conditions. Hong Kong is located in 22.33Nº and 114.17Eº with a cooling degree day (CDD) of 1976 and heating degree day (HDD) of 237. The monthly average outdoor temperature in the hottest month (i.e. July) is 28.9 ℃

and that for the coldest month is 16.1 ℃. Above temperatures are well within the applicability of the ASHRAE55 Adaptive Comfort Model (ACM) (de Dear and Brager, 2002).

2.1.2. Construction of generic model

The generic model (see Fig. 3) used for the simulation-based design optimization is developed from previous studies conducted by the authors to represent a typical high-rise residential building for the local low-income population (Chen et al., 2015b). The performance of the generic model in predicting indoor thermal and daylight performance under natural or mix-mode ventilation conditions has been validated by full-scale on-site measurements (Chen and Yang, 2015; Schulze and Eicker, 2013; Zhai et al., 2011). Airflow Network (AFN), daylight, thermal balance and photovoltaic generator modules are combined in the simulation platform to provide building outputs for the sensitivity analysis (SA) and optimization. The hybrid ventilation control algorithm based on the difference of indoor-outdoor temperatures and HVAC setpoints (referring to ASHRAE55 90% acceptability limits) is adopted to determine HVAC loads, ventilation rates and indoor thermal conditions, while the dimming control is adopted to determine the indoor illuminance and lighting energy consumption (Chen and Yang, 2018).

In the building model with PV applications, PV modules are assumed to be coupled with the surface heat transfer model of both transparent and opaque facades, so that the part of solar radiation converted to electricity is removed from the heat transfer through the envelope (Chan, 2018). The Simple generator model is used instead of the Equivalent One-Diode and Sandia model to efficiently predict power generation from PV envelopes and expedite the decision-making process in the initial design stage. A fixed average conversion efficiency under the standard test conditions (STC) is selected to estimate monthly and annual power supplies (Wang et al., 2017; Zhang et al., 2016). The power generation rate from a PV surface is calculated by Eq. (1):

$$P = A_s \cdot f_a \cdot G_T \cdot \eta_c \cdot \eta_i \quad (1)$$

where A_s is the area of a PV surface; f_a is the fraction of the surface with active PV cells; G_T is the incident solar radiation on the vertical surface; η_c is the PV module conversion efficiency; and η_i is the conversion efficiency of the invert.

2.1.3. Defining input design variables

Building design inputs can be divided to two categories: independent passive architectural

parameters and dependent parameters of coupled PV systems. Independent passive design parameters include the building orientation (BO), external obstruction height (EOD), external obstruction distance (EOD), wall thermal resistance (WTR), wall specific heat (WSH), window U-value (WU), visible light transmittance (VT), light-to-solar gain ratio (LSG), overhang projection fraction (OPF), window to ground ratio (WGR) and infiltration air change per hour (IACH). Among these parameters, EOD and EOH are used to address the shading effect from peripheral buildings, while IACH is used to address the uncontrolled ventilation during air-conditioned periods. As multiple studies and energy codes on domestic buildings in China and EU recommend an infiltration rate between 0.5 to 1.5 ACH for various air-tightness levels (Fernández-Agüera et al., 2016; Sfakianaki et al., 2008), its input distribution range is adjusted accordingly to represent a more realistic scenario. Thermal inertia of walls is addressed with a combination of variable wall specific heat (i.e. WSH) and thermal resistance (i.e. WTR) as well as fixed wall dimensions and densities in the EnergyPlus Model (Aste et al., 2009). Probability distributions and baseline values of all independent design variables are presented in Table 1 (ASHRAE, 2009; BEAM, 2012; Chen et al., 2018). On the other side, the solar heat gain coefficient (SHGC), active glazing PV area (GPVA), active wall PV area (WPVA) and widow opening factor (WOF) are defined as dependent variables of coupled PV systems. As mentioned in the introduction, *SHGC* can be derived from Eq. (2):

$$SHGC = \frac{VT}{LSG} = \tau + \alpha p \tag{2}$$

where τ is the directly transmitted solar radiation through the window; α is the absorbed solar radiation by the window panel; and p is the proportion of absorbed solar radiation which is eventually transferred to the indoor ambiance. LSG is varied from 1.0 to 2.4 to include design options from the reference clear glazing to triple low-e glazing (Gueymard and duPont, 2009). *GPVA* is assumed to be dependent on *VT* as defined by Eq. (3):

$$GPVA = 1 - \frac{VT}{0.9} \tag{3}$$

where 0.9 is derived from the assumption that the active PV module is opaque and the remaining window adopts glazing with 90% visible transmittance. The conversion efficiency of the window PV is set to 6.3% according to tested semi-transparent amorphous silicon glazing (Wang et al., 2017). WPVA is dependent on the window to wall ratio, and 90% of the wall area is assumed to be covered by monocrystalline silicon photovoltaic modules with a conversion efficiency of 15% (Petter Jelle et

al., 2012). The configuration of PV materials on a typical residential unit is illustrated in Fig. 3. WOF is the operable window fraction excluding the active PV area from the total window surface. This dependent variable will significantly influence the natural ventilation performance.

2.1.4. Defining other model settings

The remaining input parameters (See Table 2) of the generic model are kept constant to focus on the impact of the passive design and coupled PV systems. The internal lighting, equipment and occupant loads are specified according to BEAM Plus guidelines. The reference setpoint for the light dimming control is specified as 150 Lux based on CIBSE Code of Lighting. The IdeaLoadsAirSystem is selected to provide cooling and heating to supplement natural ventilation at a COP (coefficient of performance) of 1.0 (Gou et al., 2018). Its setpoint temperatures are dynamically updated with upper and lower limits of the ASHRAE55 90% acceptability. Operation schedules for the room occupancy, cooling, heating, lighting and miscellaneous equipment are referenced to the local building energy code and BEAM Plus guide.

2.2. Sensitivity analysis methods

2.2.1. Qualitative approach

The screening-based Morris method is adopted to conduct qualitative sensitivity estimation of selected independent design inputs in Section 2.1.This SA method can provide a preliminary estimation of the relative importance between k design variables based on the Elementary Effect (EE_i) defined as per Eq. (4) [40].

$$EE_i(x) = \frac{\left[y(x_1, x_2, \cdots x_{i-1}, x_i + \Delta, \cdots x_k) - y(x)\right]}{\Delta} \tag{4}$$

The design input space can be explored by Morris with a randomized “one factor at a time” modelling experiment at a small sampling cost. Two important statistics derived from the elementary effect is the absolute mean μ^* - indicating the main contribution of each design input to the output variation and the standard deviation σ - indicating the non-linearity and parametric interactions (Menberg et al., 2016):

$$\mu^* = \sum_{i=1}^{r} \left| EE_i \right| / r \tag{5}$$

$$\sigma = \sqrt{\sum_{i=1}^{r}(EE_i - \mu)^2 / r} \tag{6}$$

The sampling size is defined as the product of the number of trajectories r and (k+1). To alleviate the negative impact from extreme values in a small sampling size, r can be adaptively changed to improve the robustness of μ^*. Another important statistical measure is σ/μ^*, which signifies the monotonicity and linearity between input and output variables when compared with thresholds of 0.1, 0.5 and 1.0 (Garcia Sanchez et al., 2014).

2.2.2. Quantitative approach

The variance-based FAST method is further conducted to quantify the contribution of each design input and validate their ranking determined by Morris. The total model variance can be decomposed as Eq. (7):

$$V(Y) = \sum_{i=1}^{k} V_i + \sum_{j>i}^{k} V_{ij} \cdots + V_{12\cdots k} \tag{7}$$

where V_i is the unique impact of each design input on the output variation, and V_{ij} is the joint of impact of the combination of any two design inputs. Dividing Eq. (7) by $V(Y)$, correlation between different orders of sensitivity indices is acquired as:

$$1 = \sum_{i=1}^{k} S_i + \sum_{j>i}^{k} S_{ij} + \cdots + S_{12\cdots k} \tag{8}$$

where the S_i is the first-order sensitivity index which is used to quantify the relative importance of each input; S_{ij} is the second-order sensitivity index; $S_{12\cdots k}$ stands for the higher-order index for the output variance which cannot be addressed by lower order indices. The total sensitivity index S_{Ti} is then obtained by summarizing the all orders of sensitivity indices involving a specific input:

$$S_{Ti} = S_i + \sum_{j\neq i}^{k} S_{ij} + \cdots + S_{i\cdots j\cdots k} \tag{9}$$

In FAST, a multi-dimensional transformation of input space is conducted with Eq. (10), where an input x_i is transformed into a scalar $-\infty < s < +\infty$:

$$x_i = \frac{1}{2} + \frac{1}{\pi}\arcsin(\sin(\omega_i s + \varphi_i)) \tag{10}$$

The required total number of model evaluations is then determined as:

$$N = 2M\omega_{\max} + 1 \quad (11)$$

where M (usually set to 4) is the number of harmonics to sum in the Fourier series decomposition (i.e. the interference factor); ω_{max} is the maximum value among frequencies ω_i (Cukier et al., 1978; Saltelli et al., 1999). The suggested minimum sampling size for $k = 11$ is recommended as 974 according to a sensitivity study on coupled equations for complicated physics and chemistry problems (Cukier et al., 1975). Because FAST has been successfully applied in previous research as a robust sensitivity interpretation of passive design strategies (Chen et al., 2017b), a modeling experiment with 10714 samples by the fast99 function in R is used as the reference to validate qualitative sensitivity measures by Morris. Furthermore, bootstrapping with 1000 repetitions is conducted on the original dataset to evaluate uncertainties of FAST indices (Chen et al., 2017a).

2.3.Design optimization with NSGA-II and HGPSPSO

After exploring different sensitivity approaches, the obtained lighting demand, HVAC demand and PV supply from building modelling are then subject to multi-objective optimizations with the non-dominated sorting genetic algorithm-II (NSGA-II). A solution set called the Pareto Frontier is derived from the optimization with the combination of EnergyPlus and JEPlus. Trade-off between different objectives can be observed in the Pareto Frontier, where no single solution is dominating others for all objectives. NSGA-II is setup as: Population size = 22 (i.e. twice the dimension of design inputs), Crossover rate = 0.9, Mutation probability = 0.355 and Iterating generation = 100 for the convergence to global optimal solutions (Chen et al., 2018). Post-optimization analyses are also conducted to further unveil the rationale of design preferences for different optimization objectives.

The weighted sum method is then applied to the optimization process by assigning equal weightings to all energy demand (i.e. lighting, cooling and heating) and supply (i.e. PV generation) objectives. Such a weighting is based on the assumption that the annual average COP of air-conditioning is 1.0 so that both cooling, heating and lighting energy are summarized in the form of electricity (Delgarm et al., 2016). Therefore the net building energy demand becomes the univariate optimization target, which reduces the multi-objective optimization to the Mono-objective optimization (Deb, 2001). Instead of NSGA-II, the hybrid generalized pattern search particle swarm optimization (HGPSPSO) implanted in GenOpt is adopted to derive the ultimate single solution

(Wetter, 2016). A brief illustration of the working mechanism for both optimization approaches is shown in Fig. 4.

Generalized Pattern Search (GPS) algorithms can be used to obtain derivative free minimization in an optimization problem (Wetter, 2016). In this study, the optimization problem is continuously differentiable so that GPS constructs stationary accumulation points and a mech in the domain of input variables. The domain is explored based on the rule that if the objective function cannot be further decreased with current mesh points, the distance between mesh points should be reduced for future iterations. A classic GPS algorithm, Hooke-Jeeves, is combined with the particle swarm optimization (PSO) as the post-processor. The setting of Hooke-Jeeves is illustrated in Table 3. HGPSPSO can greatly increase the chance of acquiring the global minimum compared with traditional GPS.

The particle swarm optimization (PSO) belongs to swarm intelligence methods which emulate the natural behavior of bird flocks in food searching. It is a multi-agent (i.e. particle) system in which each individual acts in a certain rule leading to a collective high-performance cooperation (Kaur and Kaur, 2015). In each generation of PSO, the individual best solution (i.e. the best value obtained by a particle) is compared with the global best solution (i.e. the best value obtained by all particles) so that the velocity and position of each particle are updated according to Eq. (12) and (13) in the next generation (Delgarm et al., 2016).

$$v_i(t+1) = v_i(t) + c_1\rho_1(\mathrm{t})(\mathrm{p}_{l,i}(t) - x_i(t)) + c_2\rho_2(\mathrm{t})(\mathrm{p}_{\mathrm{g},i}(t) - x_i(t)) \tag{12}$$

$$x_i(t+1) = x_i(t) + v_i(t+1) \tag{13}$$

where t is the number of generations; $x_i(t)$ is the i^{th} particle's position in t^{th} generation; $p_{l,i}(t)$ is the position where i^{th} particle yield the best solution; $p_{\mathrm{g},i}(t)$ is the position of the best particle over all generations; c_1 is the cognitive acceleration constant (i.e. a particle attracted to its own best solution); c_2 is the social acceleration constant (i.e. a particle attracted to its neighbors' best solution); $\rho_1(\mathrm{t})$ and $\rho_2(\mathrm{t})$ are random numbers between 0 and 1 to prevent the concentration of particles in the search space and increase the diversity of solutions.

In GenOpt, PSO is further improved with the constriction coefficient $\chi(\kappa,\varphi)$ to improve its

capability in finding global optima. Increasing the constriction coefficient can expedite the convergence process and therefore improve the exploitation of the optimization. Eq. (12) can then be updated to Eq. (14) and $\chi(\kappa,\varphi)$ is expressed by Eq. (15):

$$v_i(t+1) = \chi(\kappa,\varphi)v_i(t) + c_1\rho_1(\mathrm{t})(\mathrm{p}_{l,i}(t) - x_i(t)) + c_2\rho_2(\mathrm{t})(\mathrm{p}_{\mathrm{g},i}(t) - x_i(t)) \tag{14}$$

$$\chi(\kappa,\varphi) \triangleq \begin{cases} \dfrac{2\kappa}{\left|2-\varphi\sqrt{\varphi^2-4\varphi}\right|}, & \text{if } \varphi > 4 \\ \kappa, & \textit{otherwise} \end{cases} \tag{15}$$

where $\varphi \triangleq c_1 + c_2$ and $\kappa \in (0,1]$ control the speed by which the population collapses to one point. The space can be exhaustively searched with a lower convergence speed when $\kappa = 1$. Apart from the constriction coefficient, the exploration of the search space is also modulated by velocity clamping as per Eq. (16) and (17), where a maximum velocity is imposed on the particle. The setting of PSO is summarized in Table 4.

$$v_i^j(t+1) = sign(v_i^j(t+1))\min\{\left|v_i^j(t+1)\right|, v_{\max}^j\} \tag{16}$$

$$v_{\max}^j \triangleq \lambda(u^j - l^j) \tag{17}$$

where λ is the maximum velocity gain; $j \in \{1,2,3\cdots k\}$ is the index of independent variables; u and l are the upper and lower limits of independent variables. If $\lambda \le 0$, no clamping is applied to PSO.

3. Results and discussions

This section demonstrates the influence of integrated PV applications on traditional passive architectural designs by comprehensive comparative analyses. Both qualitative and quantitative sensitivity analyses are conducted with Morris and FAST, from which the minimum required model evaluations for Morris are determined and the dimension of design space is reduced. NSGA-II and HGPSPSO are adopted to perform multi-objective and mono-objective optimizations, where the setting of PSO is subject to adaptive variations. Finally, detailed energy flows and indoor environmental conditions of optimum design solutions are analyzed and discussed.

3.1.Qualitative and quantitative analysis of design input

Morris is first used for modelling experiments with the suggested 10 trajectories as the benchmarking case. The total number of model evaluations is then estimated as 120 given the 11

independent design inputs (Menberg et al., 2016). As shown in Fig. 5, the μ^* - σ chart can be subdivided to four areas: the area under σ/μ*=0.1 indicates a linear relationship between the model input and output; the area between σ/μ*=0.1 and σ/μ*=0.5 indicates a monotonic relationship between the model input and output; the area between σ/μ*=0.5 and σ/μ*=1 indicates an almost monotonic relationship; the area above σ/μ*=1 indicates a non-linear and non-monotonic relationship. Accordingly, it can be clearly observed that passive design parameters except BO (building orientation), OPF (overhang projection fraction) and EOD (external obstruction distance) all have monotonic or close to monotonic relationship with the net building energy demand, while none of the input is linearly related to the output (Garcia Sanchez et al., 2014). These correlations proved that the most commonly used linear regression is not suitable for SA in this study. Compared to an existing study where infiltration in air-conditioned period is not considered, IACH (infiltration air change per hour) becomes the most influential design parameters instead of SHGC (solar heat gain coefficient) / VT (visible light transmittance) (Chen and Yang, 2018). The increased importance of infiltration confirmed that uncontrolled ventilation has great impact on the cooling energy use in a hot and humid climate. Such findings echo with the conclusion of a sensitivity study conducted on an apartment building in a similar climatic condition (Yıldız and Arsan, 2011).

When PV systems are coupled with the passive design as per Fig. 5b, IACH is still ranked first among all independent variables. However, the window to ground ratio (WGR) has surpassed others becoming the second important design parameter while the building orientation (BO) ranks the fourth considering the PV power generation. Their importance is attributed to dependent design variables including the active PV area in opaque and transparent surfaces which can decide the corresponding PV energy supply. It can also be noticed that the net building energy demand becomes almost monotonically correlated with BO, whereas its relationship with VT turns to be non-linear and non-monotonic. From above analyses, Morris indices can not only inform building designers the rank of design variables but also the correlation and interaction between model inputs and outputs. However, the exact contribution of each design factor and their joint influences over the building model can only be confirmed by further quantitative analyses.

Fig. 6 presents quantitative factor prioritizing results (i.e. FAST first-order indices) for both building design scenarios (i.e. with and without PV systems). In the traditional passive design case,

IACH contributes to the most variation (i.e. 36.9%) in the model output. Window optical and thermal properties (i.e. VT and LSG) account for 14.8% and 14.2% of the output variation, ranking second and third in terms of the design importance. The rest of design inputs are considered less important with a total contribution of 14.8%. Interactions of all input variables account for about 19.3% of the output variation, indicating that first-order indices alone cannot be used to consolidate an insignificant design factor. When the passive design is coupled with PV systems, IACH still ranks first among all design factors with a similar contribution of 37.5%. Instead of VT, WGR ranks second with a contribution of 14.7%. LSG still ranks third given its influence over the net building energy consumption with a slightly less contribution of 10.9%. BO, EOH and VT rank after LSG in sequence contributing to 7.3%, 6.0% and 5.6% of the output variation respectively. The contribution of interactions between design factors in this design case is however reduced to 10.9%, indicating greater individual impact from major design parameters. In both building design scenarios, WSH is close to zero with no significant unique contribution to changing the annual building energy demand. Nonetheless, it cannot be excluded in this stage because of potential interactive effects with other design factors.

To perform factor fixing for above design inputs, FAST total-order indices are calculated to identify non-influential design parameters and reduce the problem space for further optimization. As summarized in Table 5 and Table 6. Even the least important WSH shows a non-zero total-order index which indicates its interaction with other design parameters. However, after applying bootstrapping to the original dataset, WSH's 95% confidential internal contains zero with a standard deviation of 0.020 in the traditional passive design scenario. Both WSH and OPF's 95% confidence intervals contain zero with standard deviations of 0.020 and 0.021 in the case of coupled passive designs and PV systems. As a result, these "zero impact" factors are fixed at baseline levels and excluded from further building energy optimizations.

When comparing FAST total-order indices and Morris indices, it can be clearly seen that the ranking of most design factors is not consistent. This seems to contradict with statements that Morris indices should be robust counterparts for total-order indices from variance-based methods such as Sobol and FAST (A. Saltelli, 2008; Menberg et al., 2016). Such deviation might be caused by the existence of outliers and skewness in the limited modelling samples of Morris and can be solved by

increasing the number of trajectories. Gan et al. also suggested that a screening-based Morris method should employ at least 16 or 32 sampling levels and no less than 20 trajectories (Gan et al., 2014). Therefore, the number of trajectories is increased from 10 to 40 to observe the variation of sensitivity measures at a level of 16. As shown in Fig. 7, it can be proved that Morris can produce a robust factor prioritizing result with 30 trajectories.

3.2. Pareto optimal solutions for multi-objective optimization

To minimize the lighting, cooling and heating demand while maximize the PV energy production, NSGA-II is first conducted on the original design space including insignificant parameters of WSH and OPF. The convergence progress for both design scenarios are presented in Fig. 8. In the traditional passive design case, the optimization reached the convergence for the lighting and HVAC demand in the 717^{th} and 1871^{th} iteration respectively. In the integrated PV design case, the optimization achieved convergence in the 257^{th}, 1506^{th} and 363^{th} iteration for the lighting and HVAC energy demand as well as PV energy supply. Statistical distributions of the energy demand within the Pareto Frontier are presented in Fig. 9 for both design scenarios.

For the building design with only passive architectural strategies, the lighting energy demand varies in relatively small range between 27.609 kWh/m^2 with an average of 28.355 kWh/m^2. The heating demand also shows minor variation with an average close to zero (0.605 kWh/m^2). The cooling energy demand, however, fluctuates in a broader range between 31.467 and 77.884 kWh/m^2, reflecting the main impact of design variables. Given the low heating demand level in the Pareto Frontier, the heating load is grouped with the cooling load as the total HVAC demand in most analyses and discussions. For the building design with integrated PV systems, the lighting, heating and cooling demands show similar distribution ranges and mean values except that the average cooling demand of these solutions is 18.464 kWh/m^2 higher in the integrated PV design case. The PV supply, varying between 9.235 and 45.091 kWh/m^2 is the other optimization objective which is highly influenced by changing design variables.

To further illustrate characteristics of Pareto optimal sets, 3D scattered plots are presented in Fig. 10. The cooling and lighting demand in Fig. 10a show a conspicuous trade-off conflict where the two objectives cannot be simultaneously minimized. A similar trade-off can also be observed from the

projection of Pareto optima on the cooling and heating plane. However, due to the negligible heating demand as shown in Fig. 8, this conflict has minor impact on the design optimization process. Furthermore, Fig. 10b illustrates another conflict between maximizing the PV energy production and minimizing the lighting demand. Unlike the above trade-offs, the project of Pareto solutions on the PV supply and HVAC demand plane indicate a possibility of synergy, by which the HVAC demand can be reduced with increased power generation.

To perform a further investigation on the configuration of design variables within the Pareto Frontier, violin plots in Fig. 11 are used to statistically summarize its underlying structure and distribution quartiles and densities. Such an expert post-Pareto analysis can elaborate the pragmatic meaning of design options so that the guidance to further optimizations and validation of initial sensitivity analysis can be provided to decision-makers (Méndez Echenagucia et al., 2015).

Fig. 11a illustrates the distribution of the design space for Pareto solutions of the passive design scenario. Design variables including OPF, BO, IACH, WTR, WSH, EOD and LSG are all concentrated around their respective mean values (i.e. circles in the middle of boxplots). Its Pareto optima show a clear design preference of a high light-to-solar gain ratio (i.e. an average of 2.239), greater distance from external obstruction (i.e. an average of 83.986 m) and larger thermal inertia (i.e. an average of 1657 J/kg K), while a low infiltration rate (i.e. an average of 0.548 ACH), small wall thermal resistance (i.e. an average of 0.446 m^2 K/W) and a short overhang projection (i.e. an average of 0.086). Optimal building orientations assemble around 148 (i.e. facing southeast) with an almost normal distribution. Echenagucia et al. suggested that narrowly distributed design variables in Pareto solutions should be fixed in the optimization to expedite convergence while widely spread variables should be treated as important design input [49]. However, this suggestion only works with WSH in this study, as it has already been regarded as an insignificant design factor in the initial sensitivity analysis. Other parameter such as IACH and LSG are also identified as important variables for the optimization problem, whereas their distributions are restricted to a narrow range. Furthermore, although widely spread in their distribution ranges, WU, WGR and EOH are identified as less important design factors by their sensitivity indices.

Compared with Fig. 11a, Pareto optima in Fig. 11b only show strong design preference for four parameters including VT, EOH, OPF and BO. The optimal building orientation generally shifted

towards south for about 30° for maximizing PV power generation. Less shading with an average OPF of 0.081 and less external obstruction with an average peripheral building height of 7.454 m are also consistent with the objective of increasing the unitization of solar energy. A contradiction with Echenagucia' s recommendation is also observed from the random distribution of WSH given its insignificant influence over the optimization performance.

3.3. Determining the optimum solution with PSO

As one intention of this study is to explore the extent to which the integrated building design can approach the near-zero energy demand target, the weighted sum method is applied with HGPSPSO to conduct an equivalent mono-objective optimization of the net building energy demand. Based on identical energy values, equal weightings are assigned to different objectives to reduce the dimension of the problem space.

When optimizing with the original design space, an adaptive variation of particle numbers is simultaneously conducted to investigate its influence over the convergence performance. As shown in Fig. 12, the net building demand (i.e. summing up the cooling, heating, lighting, equipment energy demand and PV energy supply) can converge to a minimum value of 61.041 kWh/m^2 at the 744th iteration with a baseline swarm size of 10. When the swarm size is increased to 20, the optimized net building energy demand of 54.319 kWh/m^2 is obtained at the 839th iteration with an increase of 12.77% computation time. After the swarm size is further increased to 40 and 80, much larger numbers of iterations of 1119 and 1716 are required to reach the same optimum solution. As a result, 20 particles are deemed sufficient for obtaining the minimum optimization objective when the number of input variables is 11. The convergence of HGPSPSO is generally faster than that of NSGA-II when comparing Fig. 12 with Fig. 8. The above finding also echoes with an existing conclusion that the convergence of PSO is slowed down by larger swarm sizes (Chen et al., 2015a). It is also proved that the swarm size can influence solution accuracy under a certain dimension of input variables.

In addition, the optimization is conducted with a reduced dimension of input variables by excluding non-significant parameters of WSH and OPF based on preliminary sensitivity analyses (See Fig. 13). The same minimum net building energy demand is achieved at the 769th iteration with 10 particles, leading to a further 8.34% reduction of computation time compared to the optimization

conduced on the original design space. Therefore, 10 particles are considered adequate to reach the optimum solution when the input dimension is reduced to 9 variables. This also indicates a potential correlation between the input dimension and required swarm size, which is subject to further investigations in future studies.

3.4.Optimum design solutions and building performance indicators

Final optimum solutions based on the weighted sum method for both building design scenarios are summarized in Table 7. The total energy demand in the passive design only scenario converged to a minimum of 90.189 kWh/m^2, including a lighting demand of 29.484 kWh/m^2, a cooling demand of 32.326 kWh/m^2, a heating demand of 0.057 kWh/m^2 and a constant equipment demand of 28.322 kWh/m^2. Its design solution consists of a low visible light transmittance (VT) and external obstruction angle (EOA) while a high window to ground ratio (WGR), light-to-solar gain ratio (LSG), wall thermal resistance (WTR) and window heat transfer coefficient (WU). The major facade is determined to be southwest-facing with a high air-tightness level (IACH). The total building demand, especially the cooling demand is slightly higher than the optimum solution derived from the previous research, in which the uncontrolled infiltration in air-conditioned period is not taken into consideration (Chen and Yang, 2018). The increment mainly comes from the extra load caused by processing external hot and humid inlet air. Compared with the baseline case in the local green building guideline, up to 52.37% building energy demand can be saved by the optimized configuration of passive architectural parameters. When the PV system is incorporated into the optimization, the major difference in the optimum solution lies in the greatly increased VT and decreased WGR, leading to an additional cooling load of 12.474 kWh/m^2. Nonetheless, the 44.800 kWh/m^2 power generation from PV systems contributes to a net reduction of the energy demand to 54.237 kWh/m^2, which helps achieve a total energy saving of 71.36% with reference to the baseline case in Hong Kong's weather condition. VT and WGR are the two critical factors influencing the dependent parameters – the active area of opaque and transparent PV modules. These parameters can cause trade-offs between the lighting, cooling and power generation. In the finalized optimum design, power generation is maximized at a cost of reduced natural ventilation and increased solar heat gain, which are further discussed in the following breakdown of building energy and indoor environmental

performances.

The monthly energy demand and supply for both building design scenarios are presented in Fig. 14. For an optimized passively designed building, the cooling energy demand only occurs between May and September with a peak load of 14.3 kWh/m^2 in July. Lighting and equipment energy demands are relatively stable with a monthly average of 4.82 kWh/m^2 in total across the typical climatic year. In contrast, monthly cooling demands in the case of integrated PV design are generally higher than those in the traditional passive design case by around 2.02 to 3.25 kWh/m^2, while lighting and equipment energy demands are almost kept at the same level. Contrary to variation trends of monthly cooling demands, monthly PV power generation peaks in December with 5.97 kWh/m^2 and reaches the valley with 2.61 kWh/m^2 in June. Therefore, the PV energy supply can reduce the annual net energy consumption of the building by a high ratio of 47.09% whereas the peak monthly building load can only be reduced by 18.83%, leading to a mismatch between the building energy demand and supply. Such building energy performance clearly indicates the necessity of adopting power storages or alternative renewable energy systems so that the near-zero energy building target can be further approached.

Energy flows of the optimum solution for both building design scenarios are presented in Fig.15. By comparing the monthly heat flow through the building envelope, it can be found that the major difference lies in the window heat loss, ventilation heat removal and heat transfer through the opaque surface. The optimum solution for the integrated PV design has a relatively larger heat loss through opaque surfaces despite the same thermal insulation level (as per Table 7), because of its larger wall area based on a smaller window to ground ratio. The monthly window heat loss in the passive design only case is apparently larger due to the higher window U-value in the optimum solution. The larger window area in the passive design only case however contributes to the higher ventilation heat removal in the cooling period.

In terms of the indoor environmental performance as shown in Fig. 16, the monthly infiltration/ventilation rate is apparently much higher during the cooling period for the passive design only case. Such an average ventilation/infiltration rate of 19.67 ACH in summer (i.e. from May to September) brings a higher thermal comfort satisfaction ratio (i.e. the time ratio of a typical year when indoor thermal comfort can be achieved) and a correspondingly less cooling energy demand. The

increased ventilation is mainly derived from the larger window area as specified in Table 7. Nevertheless, a mismatch between the natural ventilation availability and cooling demand can still be observed as the bar chart shows the lowest ventilation/infiltration rate in the hottest month (i.e. July). Unlike and the thermal comfort and ventilation performance, the daylight satisfaction ratio is consistent in the two design scenarios with an annual average of 74.25% and 75.29% respectively. The consistence is derived from the covariation of two design parameters: the visible light transmittance and window to ground ratio. Although the optimum case for the integrated PV design is characterized by a smaller window area, its visible transmittance is higher to balance the daylight availability. This situation stands for a typical interactive effect between different design parameters.

4. Conclusions

This article presented a comparative simulation-based optimization study on the passive building design with and without integrated PV systems. A joint modelling platform consisting of EnergyPlus, JEPlus, R and GenOpt is developed to conduct different sensitivity and optimization analyses with adaptive variation of key parametric settings. Priorities of independent design parameters and their optimal configurations in optimal solutions are determined for the hot and humid climate with a simultaneous consideration of reducing building demands and increasing renewable power supplies. Major findings are detailed as below:

1) PV modules are coupled with the surface heat transfer model of opaque and transparent envelope facades so that the converted solar radiation was removed from the heat transfer through the envelope. Dependent input variables including the active PV area, solar heat gain coefficient and widow opening factor were dynamically coupled with independent passive design parameters including the window to ground ratio (WGR), visible light transmittance (VT) and light-to-solar gain ratio (LSG). The window area without solar cells was controlled with previously proposed hybrid ventilation strategies based on the ASHREA 55 adaptive comfort model. From such coupling mechanisms, the integrated PV and passive design modelling platform was proposed for global design optimizations.
2) Both qualitative and quantitative factor prioritizing was conducted on traditional passive design and integrated PV design cases. Based on Morris indices with a small reference sampling size, non-linear but almost monotonic correlations between model inputs and outputs were identified

by σ/μ* ratios. In both building design scenarios, the envelope air-tightness (i.e. IACH) was constantly considered the most important design parameters for the building energy performance. The window LSG ranked directly after IACH for a traditional passive design but was replaced by WGR when PV systems are coupled to the design. The combination of qualitative and quantitative analysis can be applied as an efficient and robust sensitivity analysis tool for not only building design optimizations but also other energy system studies.

3) Given 19.3% and 10.9% interactive effects of design parameters identified from the factor prioritizing process, FAST total-order indices were further calculated to perform factor fixing by the bootstrapping strategy. The 95% confidence levels for each design parameters are obtained based on their respective standard deviations to search for potential zero-valued indices. The wall specific heat (WSH) for the passive design only case while WSH and OPF for the coupled PV and passive design case were accordingly excluded from the list of significant design factors. In addition, the ranking of design factors by Morris indices managed to reach a consistency with that by FAST total-order indices when the minimum required number of trajectories was satisfied.
4) Multi-objective optimizations based on NSGA-II were conducted for both building design scenarios to obtain Pareto optimal solutions. Trade-offs between the cooling and lighting demand as well as between the lighting demand and PV supply were clearly observed from the statistics of optimization objectives. A post-Pareto analysis was also conducted to reveal the underlying statistical structure of design input configurations. It was indicated that a broad distribution in the definition domain can refer to an insignificant design variable in the optimization process.
5) Mono-objective optimizations with HGPSPSO were further conducted to acquire the final optimum solution for minimizing the net building energy demand, which turned out to be 54.237 kWh/m^2 with 10 particles and 9 significant design variables in the integrated PV design scenario. If using the original 11 variables for the design space, HGPSPSO can only obtained the same solution accuracy when the swarm size was increased to 20 and the computation time was increased by around 12.77%. The optimum solution with PV systems in Hong Kong can save up to 71.36% of the energy demand compared to a reference building as per the local building standard. The main difference with the optimum traditional passive design case lies in greatly increased VT and decreased WGR, leading to a 12.474 kWh/m^2 additional cooling load while

44.800 kWh/m^2 power generation from PV systems.

6) Furthermore, monthly building energy demands, heat flows through the building envelope and indoor environmental indices were compared for both building design scenarios to validate the influence from different design configurations. Although the PV energy supply can reduce annual net energy consumption of the building by a high ratio of 47.09%, the peak monthly building demand can only be reduced by 18.83%, leading to a mismatch between the building energy demand and supply. It is thus recommended that the near-zero energy building target can be further approached by adopting power storages or alternative renewable energy systems.

Acknowledgment

The work described in this paper was supported by the Innovation and Technology Fund with project No. ITS/171/16FX and the Postdoctoral Fellow Scheme of the Faculty of Construction and Environment, The Hong Kong Polytechnic University (Grant No.: K-ZM2G). Appreciation was also given to the National Key R&D Program of China, Research and Demonstration of Key Technology of Net-Zero Energy Building (Project No.: 2016YFE0102300).

References

A. Saltelli, M.R., Terry Andres, Francesca Campolongo, Jessica Cariboni, Debora Gatelli, Michaela Saisana, Stefano Tarantola, 2008. Global Sensitivity Analysis: The Primer. John Wiley & Sons Ltd.

ASHRAE, 2009. 2009 ASHRAE® HANDBOOK FUNDAMENTALS, Atlanta.

Aste, N., Angelotti, A., Buzzetti, M., 2009. The influence of the external walls thermal inertia on the energy performance of well insulated buildings. Energy and Buildings 41, 1181-1187.

Baldi, S., Karagevrekis, A., Michailidis, I.T., Kosmatopoulos, E.B., 2015a. Joint energy demand and thermal comfort optimization in photovoltaic-equipped interconnected microgrids. Energy Conversion and Management 101, 352-363.

Baldi, S., Michailidis, I., Ravanis, C., Kosmatopoulos, E.B., 2015b. Model-based and model-free “plug-and-play” building energy efficient control. Applied Energy 154, 829-841.

BEAM, 2012. BEAM Plus New Buildings Version 1.2. HKGBC and BEAM Society Limited.

Chan, A.L.S., 2018. Evaluating the impact of photovoltaic systems on the thermal performance of buildings and its implication to building energy code. A case study in subtropical Hong Kong. Energy Policy 119, 674-688.

Chen, S., Montgomery, J., Bolufé-Röhler, A., 2015a. Measuring the curse of dimensionality and its effects on particle swarm optimization and differential evolution. Applied Intelligence 42, 514-526.

Chen, X., Yang, H., 2015. Combined thermal and daylight analysis of a typical public rental housing development to fulfil green building guidance in Hong Kong. Energy and Buildings 108,

420-432.

Chen, X., Yang, H., 2018. Integrated energy performance optimization of a passively designed high-rise residential building in different climatic zones of China. Applied Energy 215, 145-158.

Chen, X., Yang, H., Sun, K., 2017a. Developing a meta-model for sensitivity analyses and prediction of building performance for passively designed high-rise residential buildings. Applied Energy 194, 422-439.

Chen, X., Yang, H., Wang, T., 2017b. Developing a robust assessment system for the passive design approach in the green building rating scheme of Hong Kong. Journal of Cleaner Production 153, 176-194.

Chen, X., Yang, H., Zhang, W., 2015b. A comprehensive sensitivity study of major passive design parameters for the public rental housing development in Hong Kong. Energy 93, 1804-1818.

Chen, X., Yang, H., Zhang, W., 2018. Simulation-based approach to optimize passively designed buildings: A case study on a typical architectural form in hot and humid climates. Renewable and Sustainable Energy Reviews 82, 1712-1725.

Cukier, R.I., Levine, H.B., Shuler, K.E., 1978. Nonlinear sensitivity analysis of multiparameter model systems. Journal of Computational Physics 26, 1-42.

Cukier, R.I., Schaibly, J.H., Shuler, K.E., 1975. Study of the sensitivity of coupled reaction systems to uncertainties in rate coefficients. III. Analysis of the approximations. The Journal of Chemical Physics 63, 1140-1149.

de Dear, R.J., Brager, G.S., 2002. Thermal comfort in naturally ventilated buildings: revisions to ASHRAE Standard 55. Energy and Buildings 34, 549-561.

Deb, K., 2001. Multi-objective optimization using evolutionary algorithms, 1st ed. John Wiley & Sons, Chichester, New York, N.Y.

Delgarm, N., Sajadi, B., Kowsary, F., Delgarm, S., 2016. Multi-objective optimization of the building energy performance: A simulation-based approach by means of particle swarm optimization (PSO). Applied Energy 170, 293-303.

Fernández-Agüera, J., Domínguez-Amarillo, S., Sendra, J.J., Suárez, R., 2016. An approach to modelling envelope airtightness in multi-family social housing in Mediterranean Europe based on the situation in Spain. Energy and Buildings 128, 236-253.

Gan, Y., Duan, Q., Gong, W., Tong, C., Sun, Y., Chu, W., Ye, A., Miao, C., Di, Z., 2014. A comprehensive evaluation of various sensitivity analysis methods: A case study with a hydrological model. Environmental Modelling & Software 51, 269-285.

Garcia Sanchez, D., Lacarrière, B., Musy, M., Bourges, B., 2014. Application of sensitivity analysis in building energy simulations: Combining first- and second-order elementary effects methods. Energy and Buildings 68, 741-750.

Gou, S., Nik, V.M., Scartezzini, J.-L., Zhao, Q., Li, Z., 2018. Passive design optimization of newly-built residential buildings in Shanghai for improving indoor thermal comfort while reducing building energy demand. Energy and Buildings 169, 484-506.

Gueymard, C.A., duPont, W.C., 2009. Spectral effects on the transmittance, solar heat gain, and performance rating of glazing systems. Solar Energy 83, 940-953.

Kaur, A., Kaur, M., 2015. A Review of Parameters for Improving the Performance of Particle Swarm Optimization.

Lee, C., Won, J., 2017. Analysis of combinations of glazing properties to improve economic efficiency of buildings. Journal of Cleaner Production 166, 181-188.

Lee, J.W., Jung, H.J., Park, J.Y., Lee, J.B., Yoon, Y., 2013. Optimization of building window system in Asian regions by analyzing solar heat gain and daylighting elements. Renewable Energy 50, 522-531.

Lee, J.W., Park, J., Jung, H.-J., 2014. A feasibility study on a building's window system based on dye-sensitized solar cells. Energy and Buildings 81, 38-47.

Méndez Echenagucia, T., Capozzoli, A., Cascone, Y., Sassone, M., 2015. The early design stage of a building envelope: Multi-objective search through heating, cooling and lighting energy performance analysis. Applied Energy 154, 577-591.

Menberg, K., Heo, Y., Choudhary, R., 2016. Sensitivity analysis methods for building energy models: Comparing computational costs and extractable information. Energy and Buildings 133, 433-445.

Mirrahimi, S., Mohamed, M.F., Haw, L.C., Ibrahim, N.L.N., Yusoff, W.F.M., Aflaki, A., 2016. The effect of building envelope on the thermal comfort and energy saving for high-rise buildings in hot–humid climate. Renewable and Sustainable Energy Reviews 53, 1508-1519.

Pal, S.K., Takano, A., Alanne, K., Palonen, M., Siren, K., 2017. A multi-objective life cycle approach for optimal building design: A case study in Finnish context. Journal of Cleaner Production 143, 1021-1035.

Petter Jelle, B., Breivik, C., Drolsum Røkenes, H., 2012. Building integrated photovoltaic products: A state-of-the-art review and future research opportunities. Solar Energy Materials and Solar Cells 100, 69-96.

Robert, C.P., Casella, G., 2004. Monte Carlo Statistical Methods. Springer.

Saltelli, A., Tarantola, S., Chan, K.P.S., 1999. A Quantitative Model-Independent Method for Global Sensitivity Analysis of Model Output. Technometrics 41, 39-56.

Schulze, T., Eicker, U., 2013. Controlled natural ventilation for energy efficient buildings. Energy and Buildings 56, 221-232.

Sfakianaki, A., Pavlou, K., Santamouris, M., Livada, I., Assimakopoulos, M.N., Mantas, P., Christakopoulos, A., 2008. Air tightness measurements of residential houses in Athens, Greece. Building and Environment 43, 398-405.

Skandalos, N., Karamanis, D., 2015. PV glazing technologies. Renewable and Sustainable Energy Reviews 49, 306-322.

Skandalos, N., Karamanis, D., Peng, J.Q., Yang, H.X., 2018. Overall energy assessment and integration optimization process of semitransparent PV glazing technologies. Progress in Photovoltaics 26, 473-490.

Szabó, L., 2015. Effect of Architectural Glazing Parameters, Shading, Thermal Mass and Night Ventilation on Public Building Energy Consumption under Hungarian Climate. Periodica Polytechnica Civil Engineering 59, 209-223.

Wang, M., Peng, J., Li, N., Yang, H., Wang, C., Li, X., Lu, T., 2017. Comparison of energy performance between PV double skin facades and PV insulating glass units. Applied Energy 194, 148-160.

Wetter, M., 2016. Generic Optimization Program User Manual Version 3.1.1. Lawrence Berkeley National Laboratory.

Yıldız, Y., Arsan, Z.D., 2011. Identification of the building parameters that influence heating and cooling energy loads for apartment buildings in hot-humid climates. Energy 36, 4287-4296.

Youssef, A.M.A., Zhai, Z.J., Reffat, R.M., 2016. Genetic algorithm based optimization for

photovoltaics integrated building envelope. Energy and Buildings 127, 627-636.

Zhai, Z., Johnson, M.-H., Krarti, M., 2011. Assessment of natural and hybrid ventilation models in whole-building energy simulations. Energy and Buildings 43, 2251-2261.

Zhang, A., Bokel, R., van den Dobbelsteen, A., Sun, Y., Huang, Q., Zhang, Q., 2017. Optimization of thermal and daylight performance of school buildings based on a multi-objective genetic algorithm in the cold climate of China. Energy and Buildings 139, 371-384.

Zhang, W., Lu, L., Peng, J., Song, A., 2016. Comparison of the overall energy performance of semi-transparent photovoltaic windows and common energy-efficient windows in Hong Kong. Energy and Buildings 128, 511-518.

Zhou, Z., Wang, C., Sun, X., Gao, F., Feng, W., Zillante, G., 2018. Heating energy saving potential from building envelope design and operation optimization in residential buildings: A case study in northern China. Journal of Cleaner Production 174, 413-423.

Zomorodian, Z.S., Tahsildoost, M., 2017. Assessment of window performance in classrooms by long term spatial comfort metrics. Energy and Buildings 134, 80-93.

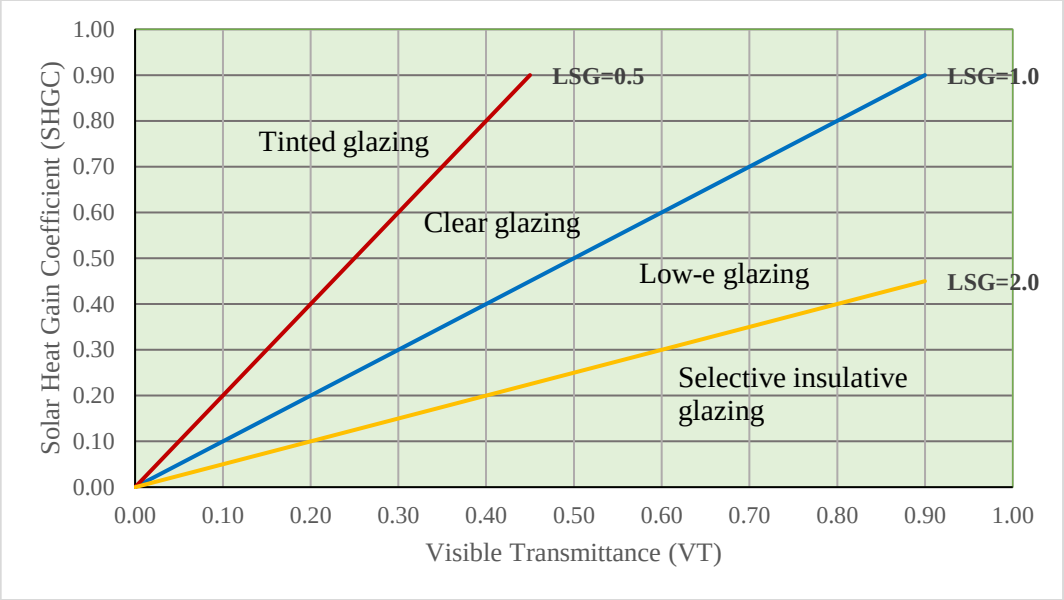

Fig. 1. Light-to-solar gain ratio distributions of common glazing [16]

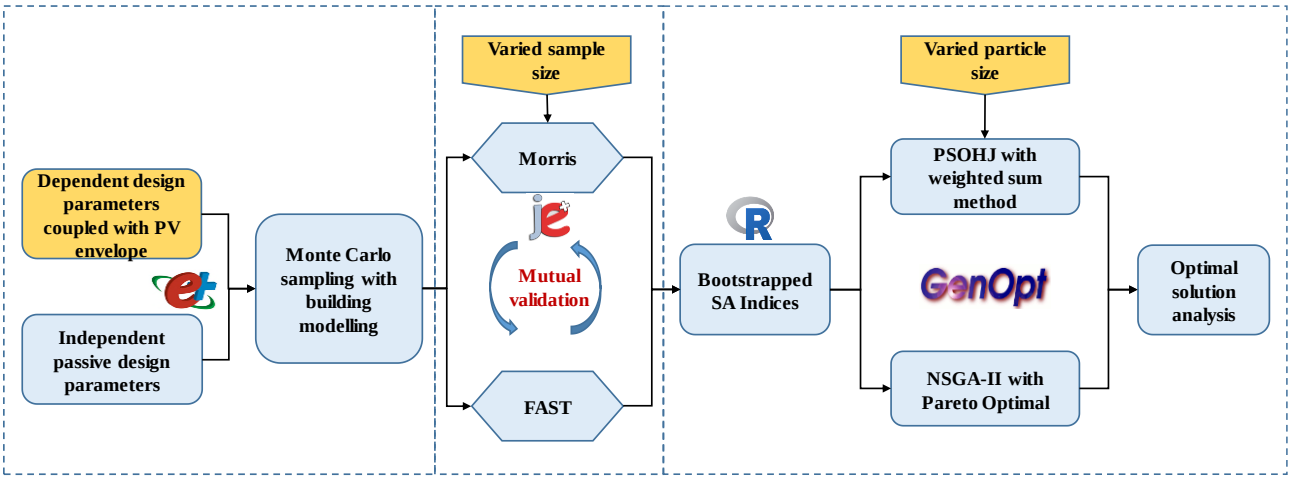

Fig. 2. Proposed research design framework

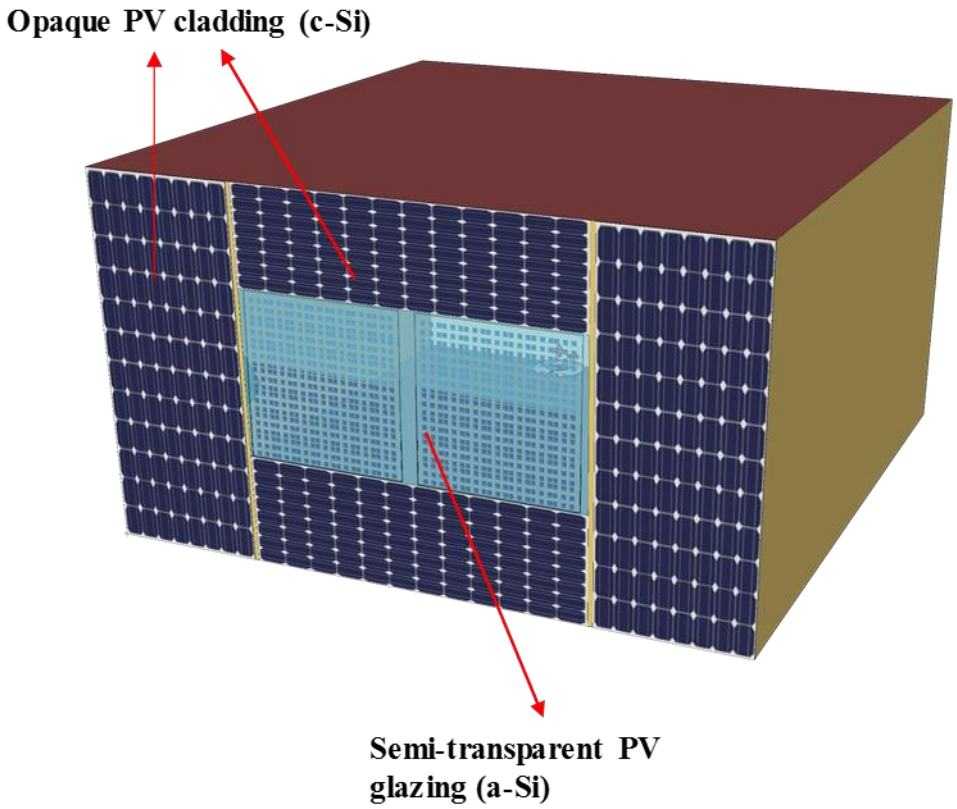

Fig. 3. Development of generic building models

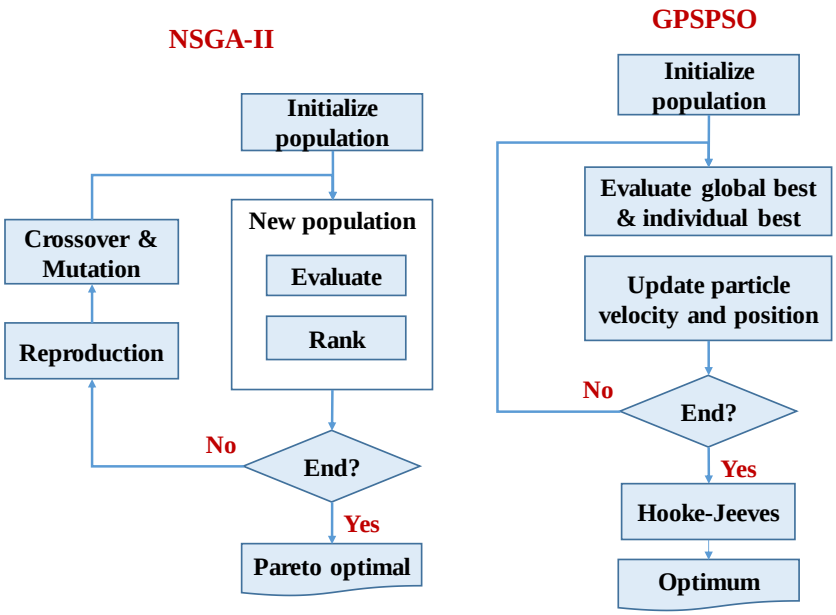

Fig. 4. Flowchart of NSGA-II and HGPSPSO

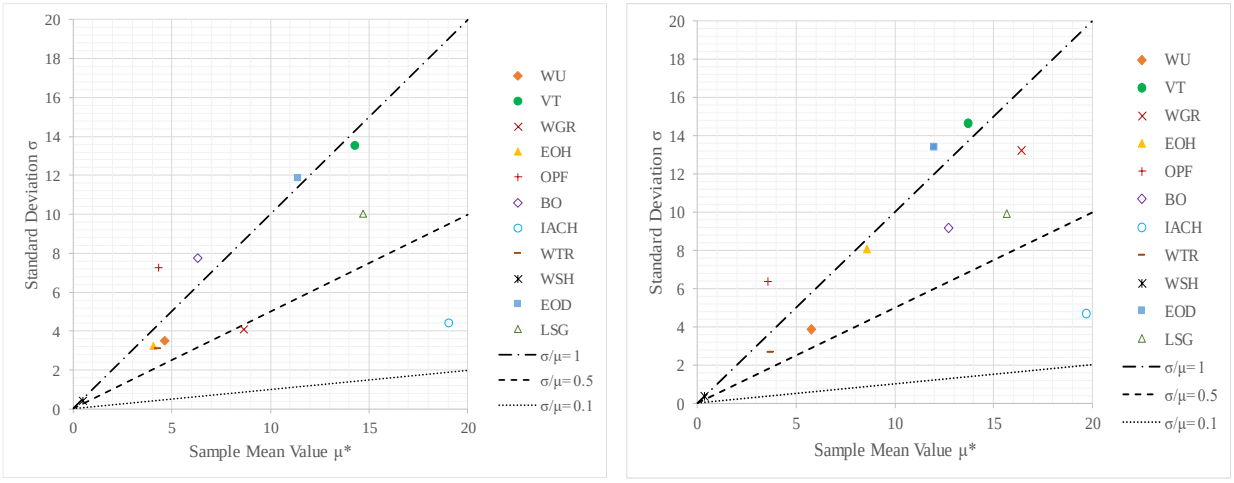

a. Passive design only b. Passive design with PV systems

Fig. 5. Morris indices for passive building design with and without PV systems

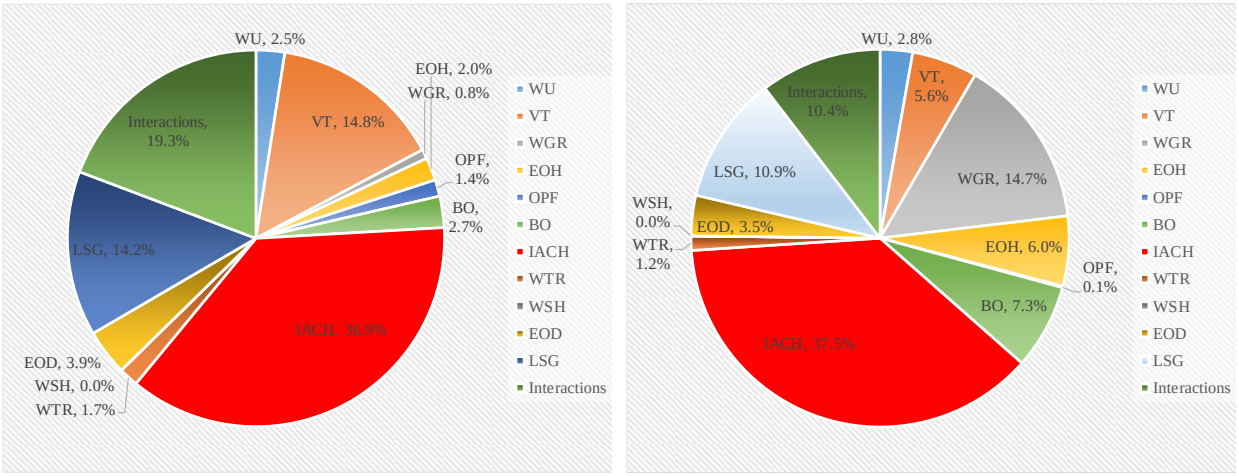

a. Passive design only b. Passive design with PV systems

Fig. 6. FAST first-order indices for passive building design with and without PV systems

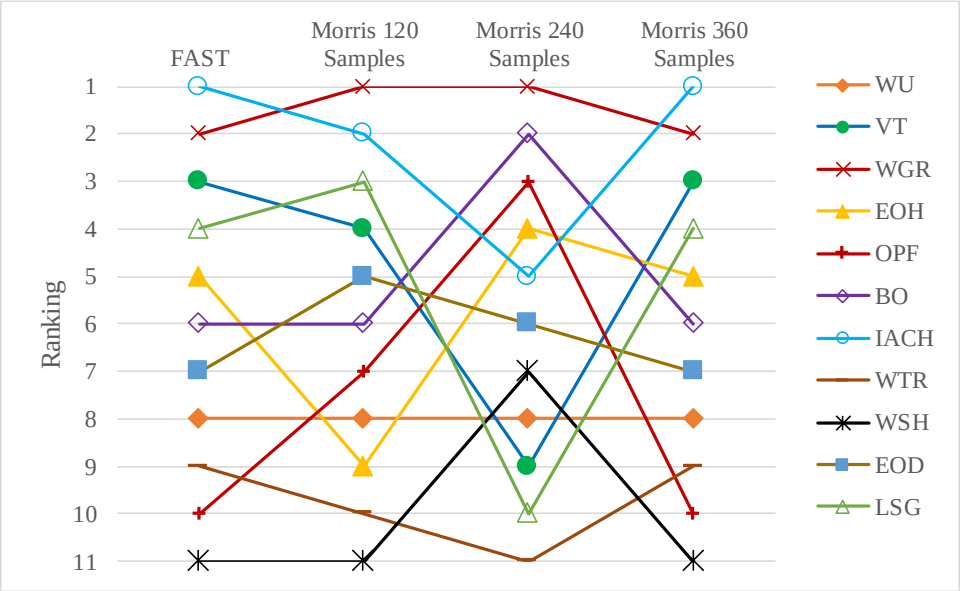

Fig. 7. Impact of trajectories on the sensitivity interpretation with Morris

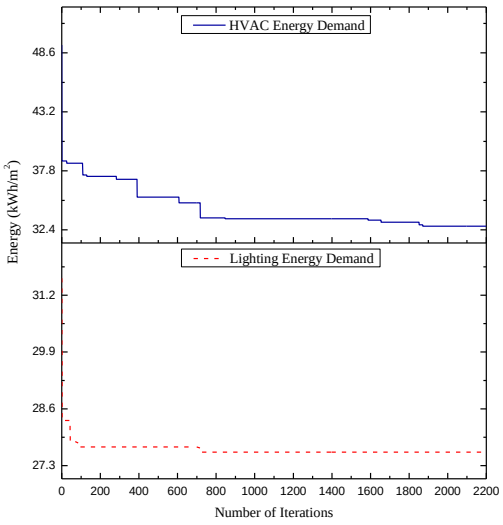

a. Passive design only

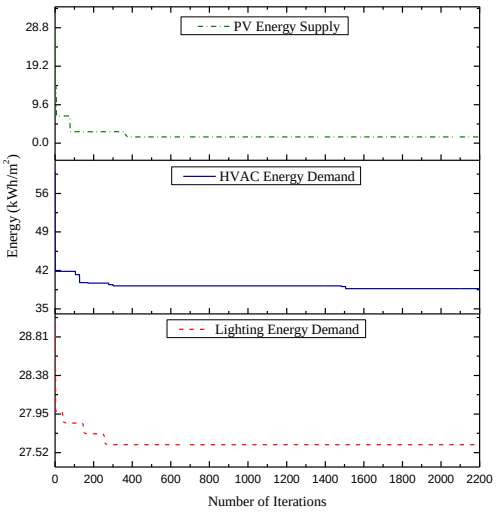

b. Passive design with PV systems

Fig. 8. Convergence progress for NSGA-II

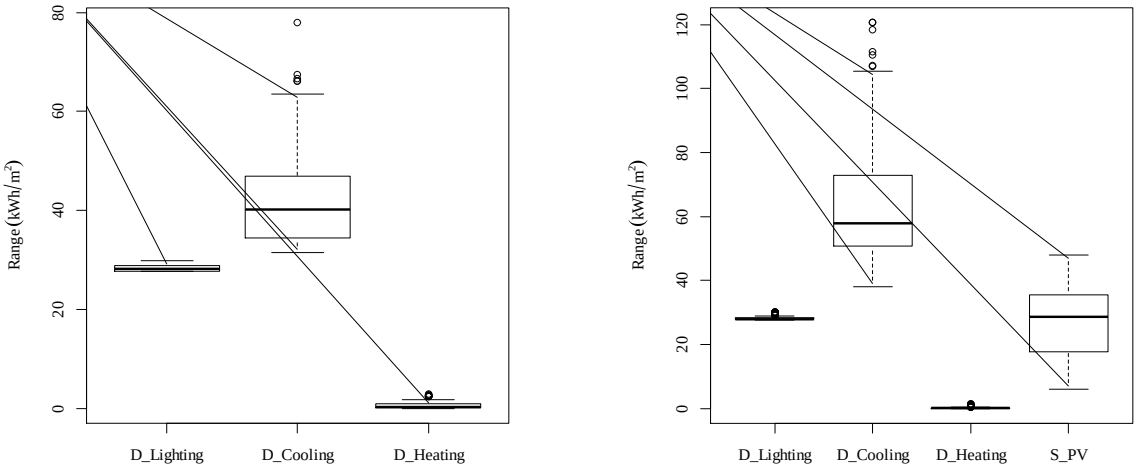

a. Passive design only b. Passive design with PV systems

Fig. 9. Energy demands distribution for Pareto optima

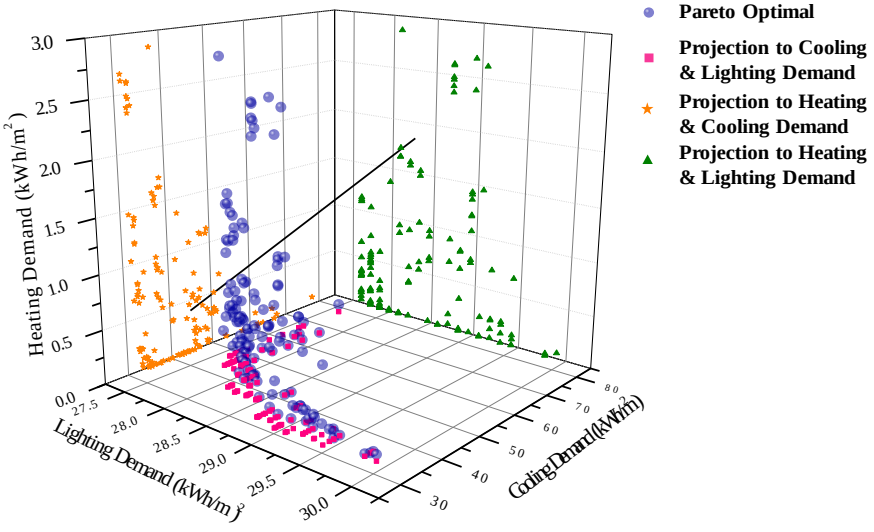

a. Passive design only

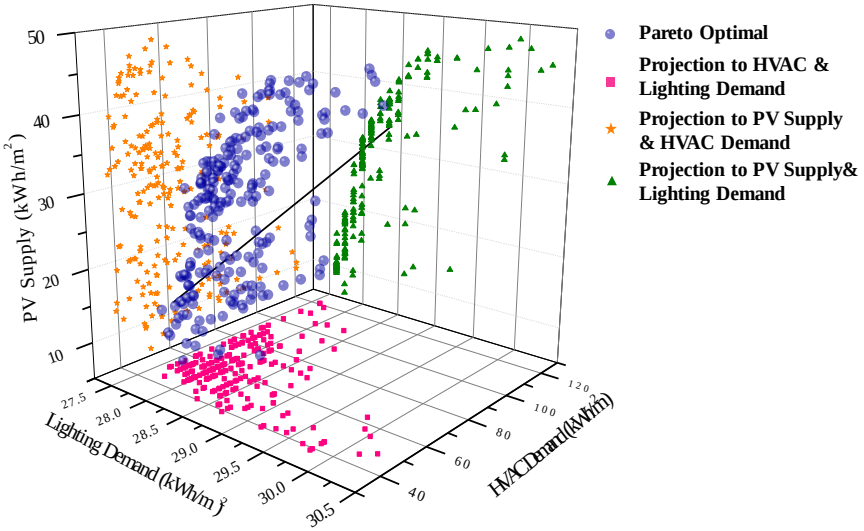

b. Passive design with PV systems

Fig. 10. 3D solution space for different objectives

a. Passive design only

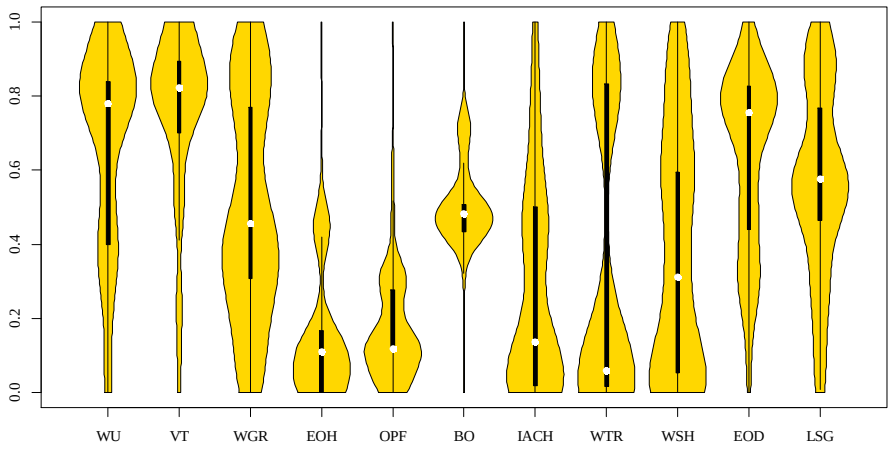

b. Passive design with PV systems

Fig. 11. Distribution of design variables for Pareto optima

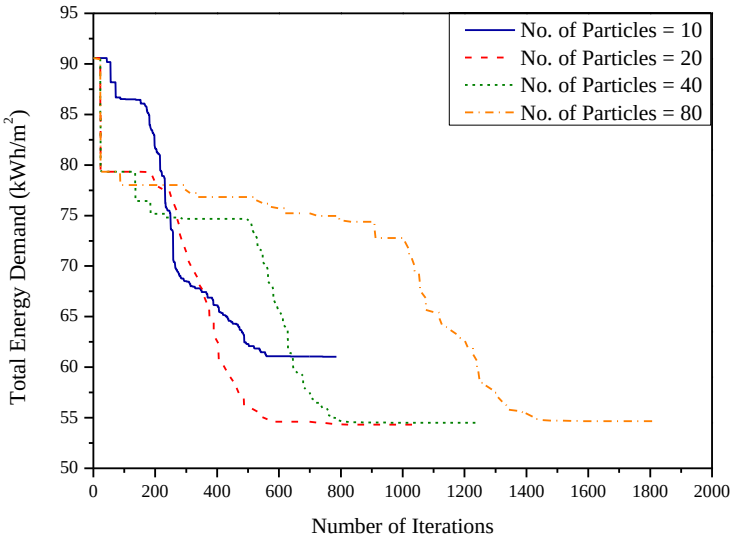

Fig. 12. Convergence progress for different swarm size of HGPSPSO

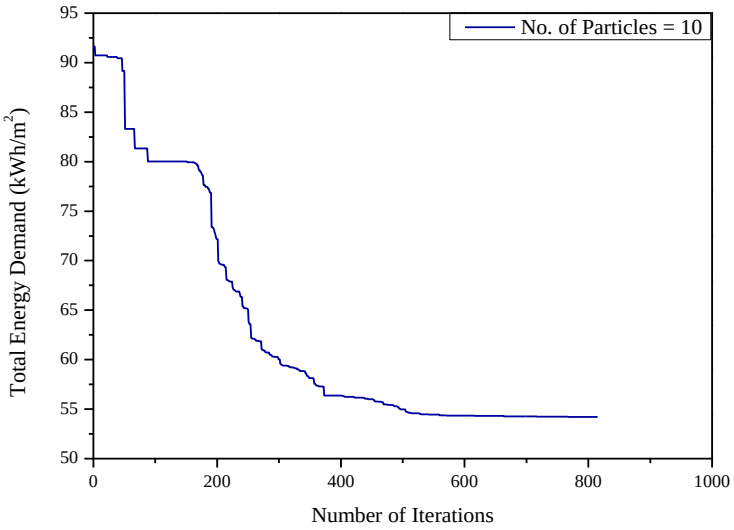

Fig. 13. Convergence progress for HGPSPSO based on simplified design space

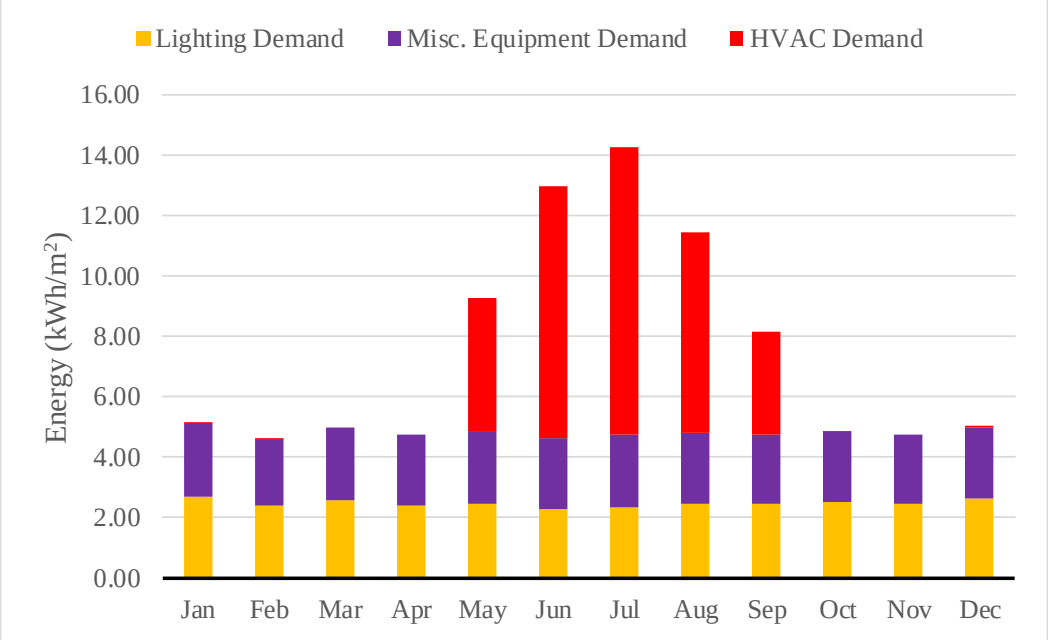

a. Passive design only

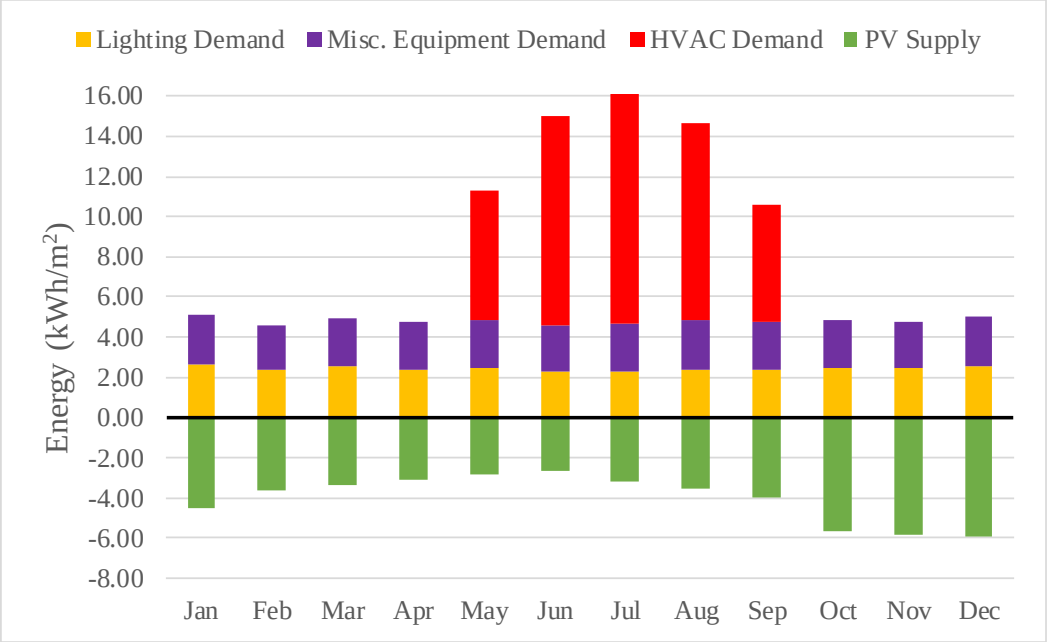

b. Passive design with PV systems

Fig. 14. Monthly variation trends of building energy demands

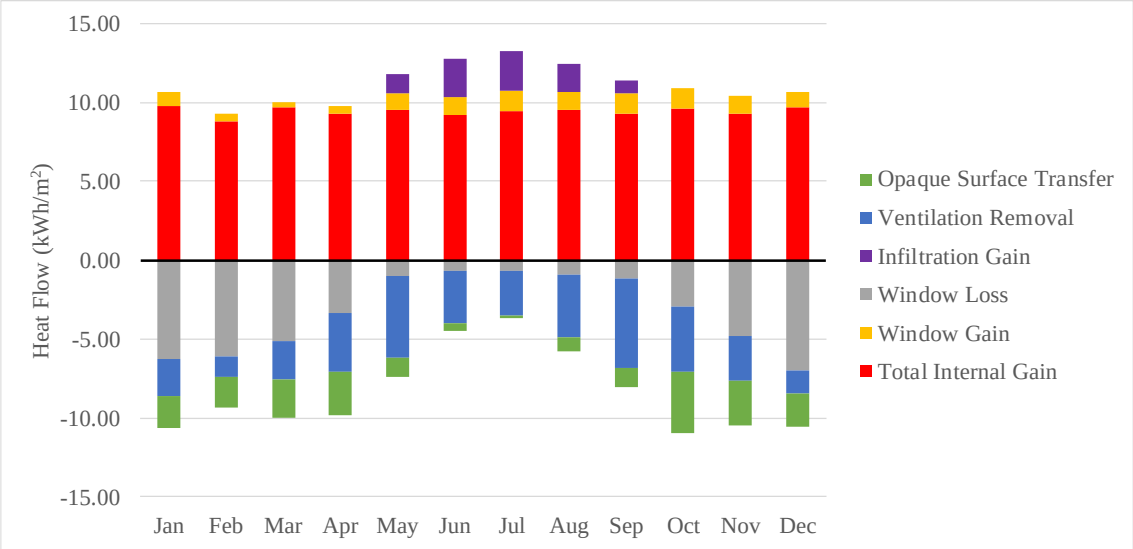

a. Passive design only

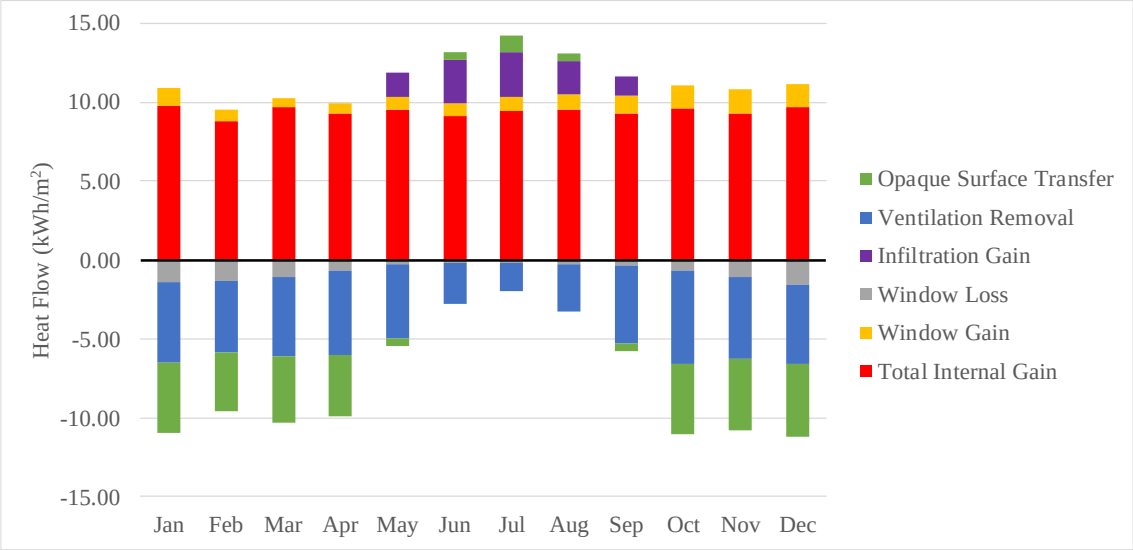

b. Passive design with PV systems

Fig. 15. Monthly energy flow through the building envelope

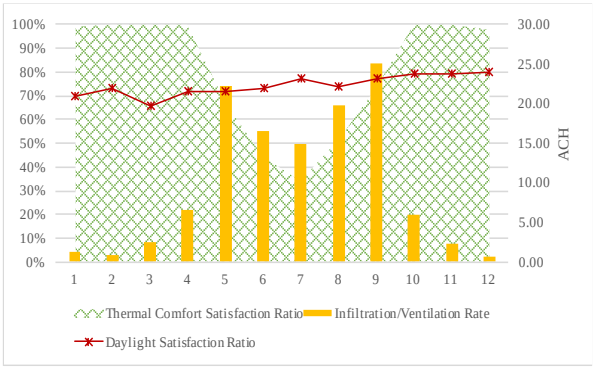

a. Passive design only

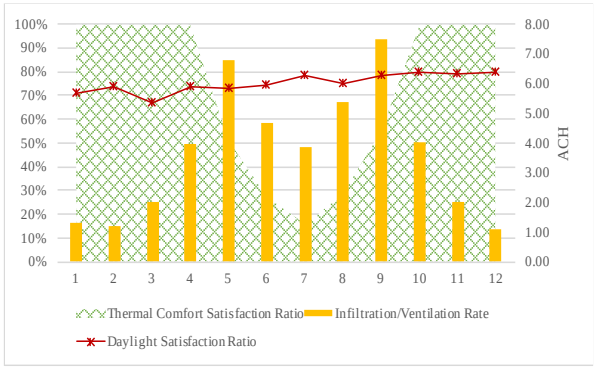

b. Passive design with PV systems

Fig. 16. Indoor environmental indices for optimum designs

Table 1. Specification of design variables

Design parameter	Value range	Distribution	Baseline value
BO (°)	0~360°	Uniform, Continuous	270
WSH (J/kg·K)	800~2000	Uniform, Continuous	840
VT	0.24~0.9	Uniform, Continuous	0.57
WTR (m^2·K/W)	0.09~6.25	Uniform, Continuous	0.09
LSG	1.0~2.4	Uniform, Continuous	1.0
WGR	0.1~0.5	Uniform, Continuous	0.225
WU (W/m^2·K)	0.2~6.0	Uniform, Continuous	5.69
OPF	0.0~0.56	Uniform, Continuous	0.00
IACH (ACH)	0.5~1.5	Uniform, Continuous	1.0
EOH (m)	0~100	Uniform, Continuous	0
EOD (m)	5~100	Uniform, Continuous	100

Table 2 Miscellaneous settings of the building model

Item	Value	Operation schedule
Occupancy	2 person/rm	All days: (1:00-8:00: 1.0, 8:00-9:00: 0.25, 9:00-20:00: 0.5, 20:00-21:00: 0.75, 21:00-0:00: 1.0)
People gain	100 W/person	
Lighting gain	15 W/m^2	All days: (1:00-7:00: 0.2, 7:00-8:00: 0.37, 8:00-14:00: 0.54, 14:00-15:00: 0.63, 15:00-20:00: 0.43, 20:00-1:00: 1.0)
Illuminance setpoint	150 Lux	
Equipment gain	142 W/rm	All days: (1:00-7:00: 0.0, 7:00-8:00: 0.3, 8:00-9:00: 0.5, 9:00-10:00: 0.3, 10:00-14:00: 0.0, 14:00-15:00: 0.5, 15:00-19:00: 0.0, 19:00-20:00: 0.5, 20:00-24:00: 0.5, 24:00-1:00: 0.5)

Table 3 Parametric setting for the Hooke-Jeeves algorithm

Parameter	Value (Integer)
Mesh Size Divider	2
Initial Mesh Size Exponent	0
Mesh Size Exponent Increment	1
Number of Step Reduction	4

Table 4 Initial parametric settings for PSO

Parameter	Value
Neighborhood Size	5
Number of Particle	10
Number of Generation	10
Cognitive Acceleration	2.8
Social Acceleration	1.3
Maximum Velocity Gain	0.5
Maximum Velocity Discrete	4
Constriction Gain	0.5

Table 5 FAST total-order indices with uncertainties for traditional passive design

	Original FAST total-order indices	Standard error	95% confidence interval lower	95% confidence interval upper
WU	0.059	0.020	0.019	0.100
VT	0.247	0.020	0.207	0.286
WGR	0.087	0.020	0.047	0.127
EOH	0.080	0.019	0.039	0.120
OPF	0.059	0.019	0.018	0.099
BO	0.080	0.019	0.039	0.122
IACH	0.399	0.019	0.359	0.439
WTR	0.054	0.019	0.012	0.095
WSH	0.025	0.020	-0.015	0.065
EOD	0.095	0.019	0.054	0.137
LSG	0.226	0.020	0.183	0.268

Table 6 FAST total-order indices with uncertainties for coupled passive design and PV systems

	Original FAST total-order indices	Standard error	95% confidence interval lower	95% confidence interval upper
WU	0.051	0.021	0.011	0.092
VT	0.183	0.020	0.143	0.223
WGR	0.310	0.020	0.271	0.350
EOH	0.151	0.021	0.111	0.192
OPF	0.026	0.021	-0.015	0.066
BO	0.143	0.021	0.101	0.184
IACH	0.400	0.020	0.360	0.440
WTR	0.051	0.021	0.009	0.093
WSH	0.022	0.020	-0.018	0.062
EOD	0.128	0.021	0.086	0.169
LSG	0.168	0.022	0.125	0.210

Table 7 Optimum solutions for both design scenarios with the benchmarking case

	Passive design only	Passive design with coupled PV systems	Base case
BO (°)	201	203	270
#WSH (J/kg·K)	840	840	840
VT	0.269	0.721	0.57
WTR (m^2·K/W)	5.799	5.556	0.09
LSG	2.4	2.4	1.0
WGR	0.417	0.10	0.225
WU (W/m^2·K)	4.32	3.42	5.69
#OPF	0.00	0.00	0.00
IACH (ACH)	0.5	0.5	1.0
*EOA (°)	9.477	2.308	0
Lighting energy demand (kWh/m^2)	29.484	29.387	36.135
Cooling energy demand (kWh/m^2)	32.326	44.800	124.092
Heating energy demand (kWh/m^2)	0.057	0.000	0.803
Equipment energy demand (kWh/m^2)	28.322	28.322	28.322
PV energy supply (kWh/m^2)	0.000	48.272	0.000
Total energy demand (kWh/m^2)	90.189	54.237	189.352

*: is calculated by arctan(EOH/EOD)

#: is fixed at the baseline value as insignificant design input